Annals of Biomedical Engineering, Vol. 42, No. 5, May 2014 (© 2014) pp. 950–959
DOI: 10.1007/s10439-014-0983-y

Assessment of Transverse Isotropy in Clinical-Level CT Images of Trabecular Bone Using the Gradient Structure Tensor

DAVID LARSSON,[1] BENOÎT LUISIER,[1] MARIANA E. KERSH,[2] ENRICO DALL'ARA,[1] PHILIPPE K. ZYSSET,[3] MARCUS G. PANDY,[2] and DIETER H. PAHR[1]

[1]Institute of Lightweight Design and Structural Biomechanics, Vienna University of Technology, Gußhausstrasse 27-29, 1040 Vienna, Austria; [2]Department of Mechanical Engineering, University of Melbourne, Parkville, VIC 3010, Australia; and [3]Institute of Surgical Technology and Biomechanics, University of Bern, 3014 Bern, Switzerland

(*Received 21 November 2013; accepted 22 January 2014; published online 29 January 2014*)

Associate Editor Umberto Morbiducci oversaw the review of this article.

Abstract—The aim of this study was to develop a GST-based methodology for accurately measuring the degree of transverse isotropy in trabecular bone. Using femoral sub-regions scanned in high-resolution peripheral QCT (HR-pQCT) and clinical-level-resolution QCT, trabecular orientation was evaluated using the mean intercept length (MIL) and the gradient structure tensor (GST) on the HR-pQCT and QCT data, respectively. The influence of local degree of transverse isotropy (DTI) and bone mineral density (BMD) was incorporated into the investigation. In addition, a power based model was derived, rendering a 1:1 relationship between GST and MIL eigenvalues. A specific DTI threshold (DTI_{thres}) was found for each investigated size of region of interest (ROI), above which the estimate of major trabecular direction of the GST deviated no more than 30° from the gold standard MIL in 95% of the remaining ROIs (mean error: 16°). An inverse relationship between ROI size and DTI_{thres} was found for discrete ranges of BMD. A novel methodology has been developed, where transversal isotropic measures of trabecular bone can be obtained from clinical QCT images for a given ROI size, DTI_{thres} and power coefficient. Including DTI may improve future clinical QCT finite-element predictions of bone strength and diagnoses of bone disease.

Keywords—Human proximal femur, Structural anisotropy, Clinical-level quantitative computed tomography, Fabric tensors, Degree of transverse isotropy.

INTRODUCTION

Osteoporosis is characterised by low bone mass and the structural deterioration of bone leading to an increased risk of bone fracture for the affected patient.[3,36] While the mechanical properties of human trabecular bone are closely related to bone mineral density (BMD),[15,16] BMD alone does not accurately assess the risk of fracture.[27] However, finite element (FE) models based on quantitative computed tomography (QCT) images are more accurate than BMD data in predicting bone mechanical properties *in vitro*,[6] as well as in simulating the mechanisms of bone remodelling.[1,26] FE model results have been well-correlated ($R^2 = 0.80$–0.87) to experimentally measured values for femoral strength.[1,2,6,7] However, the correlations between model and *in vitro* results are dependent on the investigated loading scenario ($R^2 = 0.80$ for stance configuration, $R^2 = 0.85$ for side configuration).[6] One explanation for the discrepancies between model and experimental predictions may be the lack of anisotropic information in models of trabecular bone.[13,32] Recent investigations on vertebral bodies,[17,19] the distal tibia,[14] and the proximal femur[24] have shown improved correlations to bone strength when structural anisotropy is included in FE models compared to isotropy-based models. The increasing demand for effective models to evaluate the risk of fracture *in vivo* as well as the efficacy of clinical treatments motivate the need for improved computational models of bone.

The accuracy of structural anisotropy measurements of trabecular bone is in part dependent on the image resolution and whether or not segmented or grey-level images are used. Several mathematical models have been suggested to assess the anisotropy of trabecular bone in QCT images.[12,23,31,33,35] When segmented high-resolution data with voxel size less than 100 μm are available, the mean intercept length

Address correspondence to David Larsson, and Dieter H. Pahr, Institute of Lightweight Design and Structural Biomechanics, Vienna University of Technology, Gußhausstrasse 27-29, 1040 Vienna, Austria. Electronic mails: larsson.david@hotmail.se and pahr@ilsb.tuwien.ac.at

(MIL) method[10] is considered the gold standard for the estimation of bone anisotropy, where the spatial orientation is derived from the number of phase changes in a binarized image in relation to orientation. However, for low-resolution images like those generated from clinical QCT, the MIL is not applicable[12] and alternative methods have been explored.[23,31,34,35] While principal stress vectors have been used to estimate the main direction of trabecular bone,[32] the accuracy of this approach has not been evaluated and the method itself is computationally expensive. In contrast, the gradient structure tensor (GST) is a computationally efficient and robust method for measuring structural anisotropy in CT images, where the spatial orientation is derived from changes in grey-level between neighbouring voxels.[12] The GST-based fabric tensor has been shown to successfully measure the principal direction of femoral trabecular bone to within 10° in 95% of μCT datasets when compared to the MIL method.[12,30,31] The degree of anisotropy between GST-based and MIL-based measurements has also been well correlated in μCT data.[12] When applied to clinical-level CT, the accuracy of measurements of the principal direction and degree of anisotropy degraded[12,37]; however, the error in the principal direction was shown to decrease with increasing degree of transverse isotropy (DTI), with DTI calculated according to Eq. (1) following the definition of Kersh *et al.*,[12] where λ_i ($i = 1, 3$) represent the eigenvalues of the tensor of interest ($\lambda_1 \geq \lambda_2 \geq \lambda_3$). Note that the DTI reflects the transversely isotropic nature of a structure, with highly transversely isotropic structures experiencing large DTI values and vice versa.

$$\mathrm{DTI} = \frac{2\lambda_1}{\lambda_2 + \lambda_3} \tag{1}$$

One possibility for improving computational predictions with minimal computational cost is to incorporate transversely isotropic parameters. We hypothesised that a threshold of DTI exists and can be used to distinguish in which specific regions of trabecular bone the principal main direction and DTI can be accurately calculated.

The overall goal of this study was to investigate the relationship between DTI and the accuracy of GST-based predictions of structural anisotropy in clinical-level QCT images of trabecular bone. The first specific aim was to develop a relationship between the GST and gold-standard MIL eigenvalues in order to achieve a direct correspondence between these two measures. The second specific aim was to investigate the sensitivity of this relationship to the region-of-interest size used to calculate the principal direction and DTI. Varying-sized cubes were segmented from high resolution-peripheral QCT (HR-pQCT) and clinical-level QCT data of cadaveric femora and used to calculate the MIL and GST tensors in each respective dataset. The MIL-based measurements of the principal direction and DTI in HR-pQCT data were used as the gold standard against which the GST-based measurements were compared.

MATERIALS AND METHODS

Specimens and Image Processing

Twelve cadaveric proximal femora from seven male and five female donors (average age = 75 ± 9.38 years) were scanned using three imaging modalities. First, dual-energy X-ray absorptiometry (DXA) data were acquired (Discovery QDR, Hologic Inc., USA) and used to calculate the total areal BMD. Each specimen was scanned with a calibration phantom (BDC Phantom, QMR Gmbh, Germany) in a QCT scanner (Brilliance64, Philips, Germany; intensity: 100 mA; voltage: 120 kV; voxel size: 0.33 × 0.33 × 1 mm^3; filter type: B (+0.5 enhancement). To avoid potential errors as a result of differences in sample positioning, all samples were qualitatively oriented with the femoral shaft parallel to the axis of the QCT scanner. The QCT scans were re-scaled to an isotropic voxel size of 0.33 × 0.33 × 0.33 mm^3. HR-pQCT data were also acquired (Xtreme CT, Scanco, Switzerland; intensity: 900 μA; voltage: 60 kV; voxel size: 82 × 82 × 82 μm^3). All scans were performed with the bones submerged in 0.9% NaCl solution to simulate the surrounding soft tissues, and a vacuum procedure was used to remove residual air bubbles.

Within both the QCT and HR-pQCT data, cubic regions of interest (ROI) spanning a range of side lengths (5, 7.5, 10 and 15 mm) were identified and aligned (Fig. 1). Only those ROIs that were completely within the trabecular region were used, based on applying a QCT-mask of the cortical bone, acquired using the procedure reported by Kang *et al.*[11] The registration of the two image sets was performed in the following manner: The QCT-images were masked to exclude the cortical bone. The cortical bone in the HR-pQCT scans was similarly masked according to the procedure reported by Pahr and Zysset.[18] After masking, a rigid transformation between the masked sets of QCT and HR-pQCT images for each femur was calculated with an image processing software (Slicer3D[8,20,21]), and used to align the femoral data identified within the QCT to the femoral data of the HR-pQCT data (thus subsequently aligning the set of ROIs to each other, Fig. 1). In order to increase the number of ROIs, the cropped cubes were allowed to overlap by half the ROI size in all orthogonal spatial directions.

MIL and GST Calculations

The main anisotropic direction was calculated in each cubical ROI, and for each ROI size, in both datasets using different fabric tensors (see Fig. 1). In order to compute the MIL fabric tensor, the HR-pQCT images were first segmented and binarised into

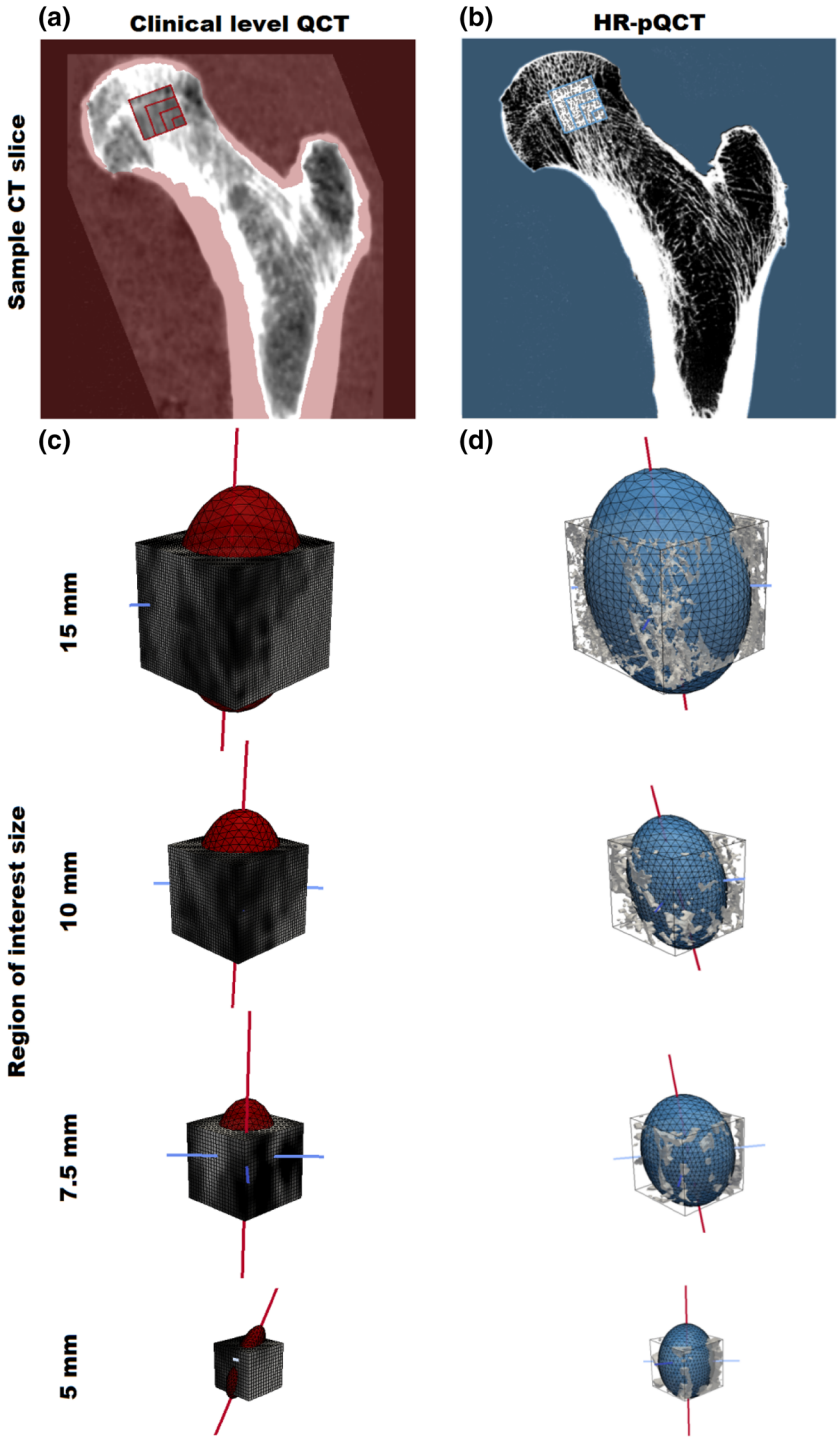

FIGURE 1. An illustrative description of the ROI size-cropping algorithm, with MIL and GST fabric tensor distributions visualized as ellipsoids with marked axis directions (main direction in red) from the QCT and HR-pQCT-scan images respectively. (a–b) Frontal sections of QCT and HR-pQCT registered images with corresponding cropped cubes in the femoral head. The red area denotes the QCT trabecular bone masked area, the blue area the masked area in the HR-pQCT. (c) Spatial representation of GST fabric tensor from the QCT model with decreasing ROI size (15 mm at the top, decreasing downwards). (d) Spatial representation of MIL fabric tensor from the same region within the HR-pQCT model with decreasing ROI size (15 mm at the top, decreasing downwards).

values of zero and one. A Gaussian filter ($\sigma = 1.2$; $r = 2$ voxels) was applied to reduce high frequency noise using a gradient-based segmentation technique.[25] An optimal single-level threshold procedure was used to obtain the final segmentation.[22]

The MIL fabric tensor of each cube was calculated from the MIL distribution function[22] based on the fabric tensor, $\boldsymbol{H}$, defined by Cowin,[5,10] and then normalised resulting in a dimensionless MIL fabric tensor, $\boldsymbol{M}$ (Eq. (2a)).[38] The dimensionless MIL fabric tensor was decomposed into corresponding orthonormal eigenvectors ($\boldsymbol{m}^i$) and connected real-positive eigenvalues (m_i) ($i = 1, 3$) (Eqs. (2b), (2c)). All calculations were performed with a custom PYTHON-based software program (Medtool 3.6, Technical University of Vienna, Vienna, Austria).

$$\boldsymbol{M} = \frac{3\boldsymbol{H}}{tr(\boldsymbol{H})} \tag{2a}$$

$$\boldsymbol{M} = \sum_{i=1}^{3} m_i \left(\boldsymbol{m}^i \otimes \boldsymbol{m}^i\right) \tag{2b}$$

$$tr(\boldsymbol{M}) = \sum_{i=1}^{3} m_i = 3, \qquad m_1 \geq m_2 \geq m_3 \tag{2c}$$

The GST was calculated in each clinical-level CT ROI. The local gradient in each direction was calculated for each voxel using a finite central difference scheme. A convolution operation of the dyadic product of the local gradient vectors was used to calculate the GST, $\boldsymbol{K}$.[31] To allow for a comparison against the normalised MIL-based tensor, the GST was normalised into a dimensionless fabric tensor, $\boldsymbol{G}$, as described by Kersh *et al.*[12] (Eq. (3a)). Similar to the MIL-based tensor, the eigenvectors and eigenvalues of the normalised GST were calculated for each ROI (Eqs. (3b), (3c)).

$$\boldsymbol{G} = \frac{3\boldsymbol{K}^{\frac{-1}{2}}}{tr(\boldsymbol{K}^{\frac{-1}{2}})} \tag{3a}$$

$$\boldsymbol{G} = \sum_{i=1}^{3} g_i \left(\boldsymbol{g}^i \otimes \boldsymbol{g}^i\right) \tag{3b}$$

$$tr(G) = \sum_{i=1}^{3} g_i = 3, \qquad g_1 \geq g_2 \geq g_3 \tag{3c}$$

Calculations of the DTI and the Principal Anisotropic Direction

Within each ROI evaluated, the eigenvector associated with the largest eigenvalue was defined as the main anisotropic direction. The main anisotropic direction calculated from GST-fabric tensors was compared against the reference MIL by calculating the directional difference between the tensor eigenvectors for each ROI size. Within each cropped cube, the DTI was calculated according to Eq. (1).

Power Model Relating the MIL and GST

In order to allow a direct quantitative comparison between the MIL-based tensors, $\boldsymbol{M}$, and gradient-based tensors, $\boldsymbol{G}$, a power-based model was derived to preserve the principal direction and the normalization of the trace. The power coefficient, n, for this model and an associated threshold DTI (DTI_{thres}) were simultaneously derived.

$$\widehat{\boldsymbol{M}} = \frac{3\boldsymbol{G}^n}{tr(\boldsymbol{G}^n)} \tag{4a}$$

$$\widehat{\boldsymbol{m}}_i = \frac{3g_i^n}{tr(g^n)} \tag{4b}$$

First, the largest eigenvalue (m_1 from Eq. (2c) and g_1 from Eq. (3c)) was associated with the main anisotropic direction. A transverse eigenvalue was then calculated as the normalized average of the second and third eigenvalues (m_2 and m_3, *and* g_2 and g_3 in Eqs. (2c) and (3c), respectively) to represent the transverse direction for each tensor. A DTI_{thres} was then calculated as the lowest DTI for which a maximum of 5% of the total number of considered ROIs above the given DTI had an angular difference greater than 30° between MIL and GST principle eigenvector. The use of 30° was determined in a preliminary study in which angular differences of 10° and 20° were analysed. Only a small number of cubes (0.1% for 10° and 1.1% for 20°) were able to pass this criterion, and therefore 30° was used as the error margin for the prediction of the main trabecular direction.

The main and transverse eigenvalues from the two fabric tensors for all ROIs above DTI_{thres} were compared using a linear least-squares fit. The power coefficient, n, was accepted if the linear correlation between the eigenvalues of the ROIs above DTI_{thres} was greater than 0.96. If the linear correlation was less than 0.96, the power coefficient was adjusted through an incremental increase/decrease in power coefficient value (depending on direction of change), a new DTI_{thres} value was calculated, and the eigenvalues for ROIs above the new DTI_{thres} value were again compared. The power model was then applied to the related fabric tensor eigenvectors (Eq. (4b)).

This analysis was repeated for all cropped ROI sizes (5, 7.5, 10 and 15 mm) resulting in a different exponent

value and associated DTI_{thres} for each cube size. The sensitivity of the calculated power coefficient to changes in BMD (comparing local changes in dataset of up to ±400 mg/cm^3), gender (comparing groups of male/female) and age (comparing local changes in dataset of up to ±18 years) was investigated.

All numerical calculations were performed using custom MATLAB code (MATLAB R2012b, version 8.0, Mathworks, Natick, USA).

RESULTS

DTI Threshold

The specific threshold DTI was obtained by iteratively increasing a limiting DTI (Fig. 2a). The percentage of ROIs with an angular difference less than 30° increased with an increasing DTI_{thres} value (Fig. 2b). Using the optimized power coefficient, n, a correlation was achieved between the DTI computed from the MIL and that computed from the GST (Fig. 2c). The number of cubes evaluated (those above DTI_{thres}) ranged from 544 cubes of ROI size 5 mm to 85 cubes of ROI size 15 mm (Table 1, Row 1).

The threshold value of the DTI associated with well-aligned main trabecular direction vectors ranged from 1·33 to 1·58 across the different sized regions of interest (Table 1, Row 2 and Fig. 3b). Smaller ROI sizes required a higher DTI_{thres} to accurately measure the principal direction ($p < 0{\cdot}01$, Table 1, Row 3). However, a larger proportion of the samples were able to be accurately measured when a larger ROI size was used, and the percentage of ROIs above the DTI_{thres} increased with increasing ROI size ($p < 0.01$, Table 1, Row 3).

Regardless of ROI size, the BMD in those trabecular cubes with a DTI above DTI_{thres} was higher than the average BMD of all ROIs (182 compared to 128 mg/cm^3; see Table 1, Row 4–5).

When calculated for discrete ranges of BMD values of individual ROIs, the DTI_{thres} decreased with increasing BMD ($p < 0.01$). This trend was observed for all ROI sizes (Fig. 4a). Linear relationships between BMD and DTI_{thres} were obtained using a least square fit for each ROI size (Fig. 4b), with the coefficient of determination (R^2) for the linear fits increasing from 0.73 for the biggest ROI of 15 mm to 0.94 for the ROI of 5 mm. As observed for the full set of femora, within each BMD range the DTI_{thres} generally increased with decreasing ROI size ($p < 0.01$).

Errors in Predictions of the Main Trabecular Direction and DTI

The errors in the predictions of the main trabecular direction were non-normally distributed ($p < 0.01$) and are therefore presented as median ± median absolute deviation. The size of the ROI did not affect the median error in the prediction of the main trabecular direction when assessing ROIs above DTI_{thres} (Fig. 5). Though not significantly different ($p = 0.12$) when assessing the full dataset, 15 mm ROIs resulted in the smallest error in the main trabecular direction (27 ± 15°), whereas the 5 mm ROIs had the largest error (34 ± 19°). In contrast, for the ROIs above DTI_{thres}, the 5 mm ROIs had the smallest error (12 ± 6°) whereas the 15 mm ROIs the largest error (16 ± 6°) (Table 1, Row 6–7). Therefore, the average error in the main trabecular direction was 14 ± 6° for all ROI sizes above DTI_{thres}.

The correlation between the DTI measured using the MIL-based fabric tensor and the GST increased with increasing ROI size for all data analysed

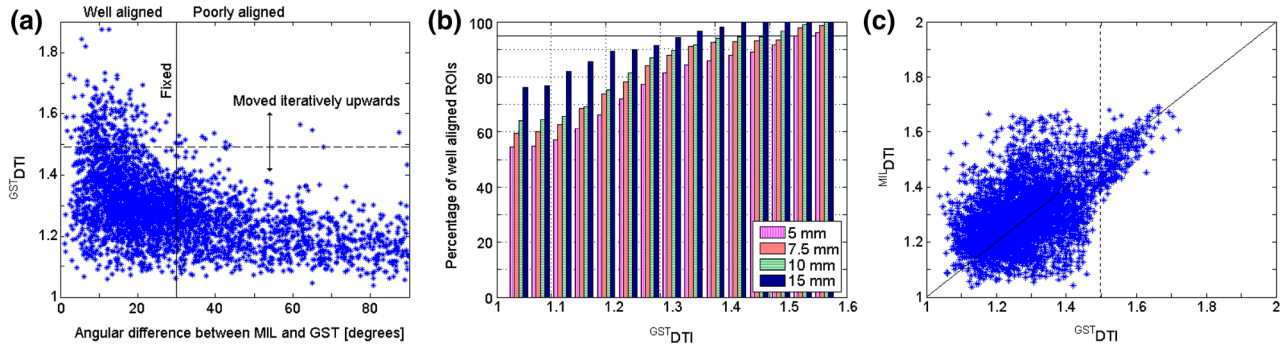

FIGURE 2. (a) DTI_{thres} Distribution of DTI against local angular difference between MIL and GST fabric tensor major eigenvectors (ROI size = 10 mm). The fixed line at 30° denotes the given border between what was defined as well and poorly aligned local regions. The dashed line illustrates the iterative process performed in order to compute a DTI_{thres}. (b) Change in the percentage of ROIs defined as well aligned as a threshold in DTI is applied. (c) Correlation between DTI originating from GST and MIL fabric tensor, respectively (ROI size = 10 mm with n according to sought correlation between MIL and GST eigenvalues. Dashed line indicates computed DTI_{thres} for given ROI size).

TABLE 1. Numerical data for DTI_{thres} and calibration coefficient n for all four ROI sizes as well as data for median angular difference and coefficient of determination between ^{MIL}DTI and ^{GST}DTI for the full set as well as for ROIs above the specific DTI_{thres}.

Row	Region of interest size (mm)	5	7.5	10	15
1	Number of ROIs above DTI_{thres}	544	380	234	85
2	DTI_{thres}	1.58	1.56	1.50	1.33
3	Percentage of ROIs above DTI_{thres}	1	4	9	27
4	BMD range for ROIs above DTI_{thres} (mg/cm^3)	216 ± 114	187 ± 86	177 ± 90	149 ± 82
5	BMD range full set (mg/cm^3)	125 ± 100	123 ± 99	126 ± 100	139 ± 100
6	Mean angular difference for ROIs above DTI_{thres} (°)	13 ± 7	12 ± 6	15 ± 6	16 ± 6
7	Mean angular difference full set (°)	34 ± 19	31 ± 17	29 ± 16	27 ± 15
8	R^2 correlation between ^{GST}DTI and ^{MIL}DTI for ROI above DTI_{thres}	0.72	0.75	0.77	0.74
9	R^2 correlation between ^{GST}DTI and ^{MIL}DTI full set	0.32	0.35	0.42	0.41
10	Power coefficient n	0.26	0.28	0.32	0.40

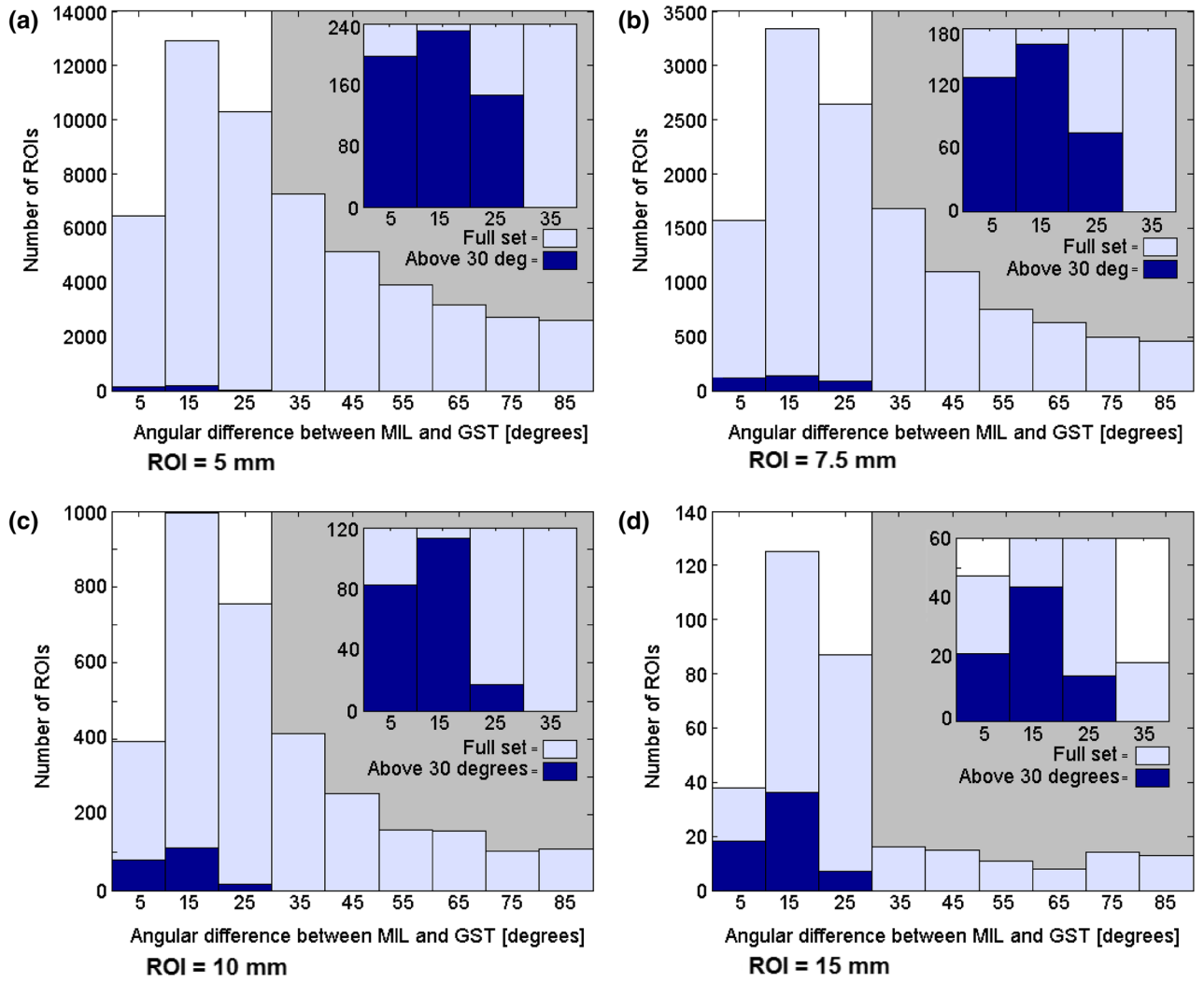

FIGURE 3. Distribution of angular differences between MIL and GST in histogram form for ROI cube size 5 mm (a), 7·5 mm (b), 10 mm (c) and 15 mm (d), respectively. Light blue area denotes the full set of ROIs, dark blue ROIs above DTI_{thres}. The grey shaded area indicates the area of an angular difference of 30° or more (defined here as poorly aligned). In the upper right corner of each figure, a sub-figure is added, providing a magnified view of the well aligned region and corresponding ROIs.

($p = 0.04$). R^2 increased from 0.32 for the smallest ROI of 5 mm to 0.42 and 0.41 for the 10 mm and 15 mm ROIs, respectively. In those regions above DTI_{thres}, the correlation did not significantly change for different sized ROIs ($p = 0.02$), with R^2 ranging from 0.72 to 0.77 (Table 1, Row 8–9).

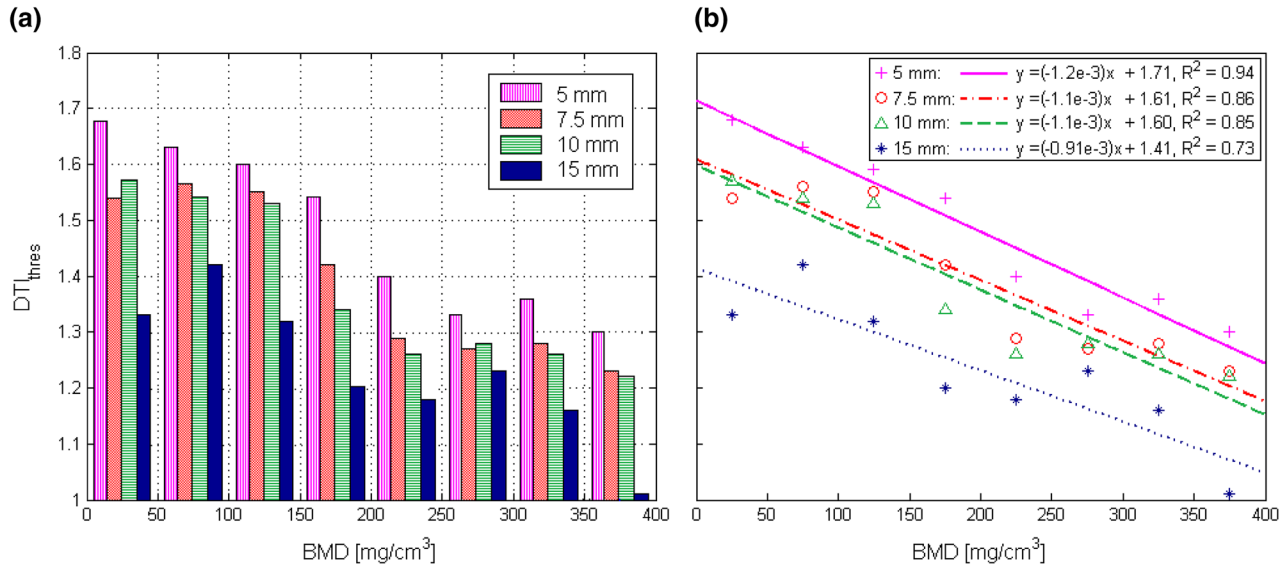

FIGURE 4. (a) DTI_{thres} for different ROI sizes when dividing dataset into slots of differently ranging BMD (most left column representing regions with BMD of 0–50 mg/cm^3, most right column representing regions with BMD above 350 mg/cm^3). (b) Linear adaption of columns in (a) using a least square fit method.

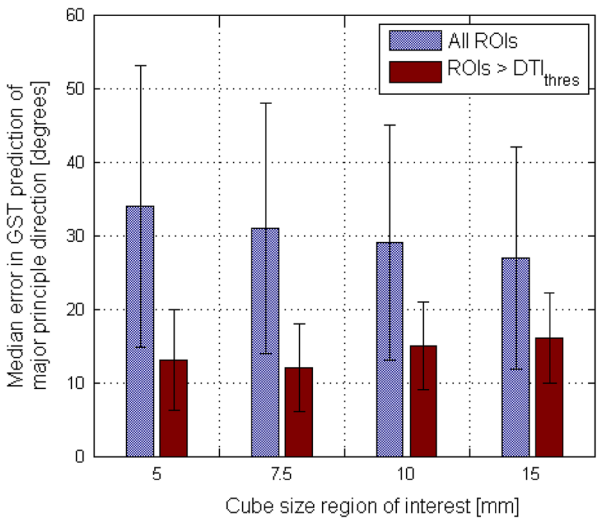

FIGURE 5. Median error in angular difference between GST and MIL prediction of main trabecular direction for all ROIs (blue dashed set) and for ROIs above DTI_{thres} (red full set, right bars).

Power Model Relating MIL and GST

The power coefficient, n, which resulted in a 1:1 correspondence of the GST and MIL for all regions above the DTI_{thres} increased with increasing ROI size (Table 1, Row 10). When increasing the ROI size from 5 mm to 15 mm cubes, the power coefficient increased from 0.26 to 0.40 for the full dataset. Using cubes above DTI_{thres}, the R^2 between the MIL and GST transversal eigenvalues for all ROI sizes was greater than 0.96. Within a given ROI size, the value of the power coefficient was not sensitive to changes in BMD (±5% upon change of ±400 mg/cm^3), gender (± 2%) or age (± 3% upon change in age of ±18 years).

DISCUSSION

The purpose of this study was to develop and evaluate a methodology for assessing the principal direction of human trabecular bone from clinical-level QCT images using the GST method. The assessment of structural anisotropy in low-resolution images is beneficial for a better understanding of bone mechanical properties and to improve the prediction of fracture load in FE analyses based on clinical images of bone.

The dependence of the correlation between the GST and the gold standard MIL method on measurements of the local DTI and ROI size was evaluated. Our results show that a DTI_{thres} value specifically calculated for each investigated ROI size can be used to evaluate the principal direction to within 30° in 95% of the regions considered. Previous studies have evaluated the ability of GST to assess directional anisotropy,[12,30,31,37] but few have applied the GST to clinical-level CT data. Wolfram *et al.*[37] presented results from a single vertebra with 36 measurement points, suggesting a good ability of the GST to assess the main trabecular direction of bone in vertebral bodies. Unfortunately, however, the ability of the GST to accurately measure the fabric eigenvalues was poor.[37] Kersh *et al.*[12] compared the GST to a Sobel structure tensor in assessing the directional anisotropy in

5·4 mm cubes of femoral trabecular bone from several donors. In their results, no significant difference between the two methods was found in assessing the main trabecular direction (median error = 28°). However, these authors recommended using the GST partly due to its computational efficiency and provided some evidence that the GST can more accurately assess regions with a high degree of anisotropy. The latter suggestion was taken and developed into a full methodology in the present study for future implementation.

We found an inverse relationship between the DTI_{thresh} and ROI size, where a decrease in region dimension was related to an increase in DTI_{thresh}. However, the accuracy of measuring DTI decreased with smaller region dimensions in the full dataset (coefficients of determination for the 15 mm and 5 mm cubes were 0·41 and 0·32, respectively). Overall, these results may reflect the nature of the QCT images, where the accuracy of the GST in estimating local properties (such as DTI) decreases as the number of evaluated voxels decreases (a change in local ROI dimension from 15 to 5 mm equals a decrease in evaluated voxels from 30,374 to 1125). The limited accuracy of the GST fabric tensor in predicting the anisotropic parameters for small ROI dimensions (i.e., 5 mm cubes) is in agreement with previous findings.[12]

When dividing the full dataset into segments of different BMD, an inverse linear relationship was obtained where values of higher BMD correlated with lower values of DTI_{thresh}. Regions of low BMD include not only fewer trabeculae but also trabeculae of reduced thickness (due to the direct relationship between BMD and BV/TV), leading to a decreased ability to assess the directional anisotropy of the specific cube using the GST. When assessing discrete BMD values for retrieved ROIs, the decreased DTI_{thresh} for cubes of higher BMD will allow more regions to be assessed as transversely isotropic as compared to using a global DTI_{thresh}. In this study, regions with a local DTI above DTI_{thresh} had increased BMD values and are, therefore, regions likely to contribute to femoral strength because of the presence of more bone.

A 1:1 relationship between the GST and MIL eigenvalues was found by introducing a calibrating power coefficient n. The n-value was dependent on cube size with a nearly linear relationship, and was insensitive to BMD, gender and age. While the sample size ($n = 12$) limits the statistical power, the dataset is thought to be representative of a mean population. The high average coefficient of determination ($R^2 = 0{\cdot}96$) underlines the robustness of the proposed model and the individual coefficients for each cube size. To the best of our knowledge, this is the first analytical relationship derived to relate the MIL and GST fabric tensors using a power function, and allows for the GST results to be integrated into existing MIL-based material models.[4,9] Attempts have been made by others to analytically relate MIL and GST to each other, proposing a linear relation between the two using a re-defined MIL-tensor originating from low-resolution images.[28] However, in the present study, the MIL was computed directly from high-resolution images and the proposed power relation is only applicable within ROIs above the introduced DTI_{thresh}, possibly explaining the discrepancy in result between the studies.

There are a number of limitations associated with the present study. First, a larger number of samples should be analysed to generalize the obtained results to a larger population as the specimens used here were from an older population. Second, previous work has shown that the detection of principal directions using GST will be to some extent dependent on the anisotropic resolution of the QCT scanner, and therefore on the positioning of the samples.[29] To limit this effect, all samples were positioned with similar orientation in the scanner. However, further work is necessary to estimate the sensitivity of the proposed method to scanner anisotropic resolution. The methodology only assesses the main direction of human femoral trabecular bone whereas bone is generally considered anisotropic. However, this study advances the state-of-the-art in assessing directional anisotropy of human trabecular bone from clinical-level CT images by providing a method with which the main trabecular direction and the DTI can be reliably calculated. Future work towards integrating these measurements into the clinical setting may provide a more accurate way of acquiring the mechanical properties of bone and enabling a detailed assessment of patient-specific fracture load and failure location. The presented methodology is able to assess regions with a sufficiently high DTI (on average 10%), and when doing so prediction errors of in average 16° may occur. However, the inclusion of DTI will likely advance the potential for accurately predicting the mechanical properties of trabecular bone compared to isotropic models. This improvement may have an important role considering the complex and multi-directional loading the femur undergoes during physiological activities (with the accuracy of isotropic models being shown to vary with loading configuration[6]). However, this speculation should be investigated in future work by estimating the improvement of computational methods such as Finite Element models that could benefit from adding local anisotropic information estimated from QCT scans. Importantly, even though a large portion of the total bone mass may not be assessed as transversely isotropic, regions of higher BMD with a pre-dominant influence on the

overall mechanical behaviour of the femur, are to a large extent included by the method. This effect might be even more pronounced in subjects experiencing low BMD e.g., young age or extreme osteoporosis, where regions of high BMD may have an even higher mechanical influence.

Generally, the information provided by the within this methodology added DTI, ROI and *n*-coefficient, may provide a crucial addition to current FE-models when assessing fracture risk, femoral strength or failure load. This might be especially the case when investigating different load configurations such as stance and side falling.

In conclusion, a new methodology has been presented to assess the principal direction of trabecular bone using the GST in clinical-level CT data of human femoral trabecular bone. Good correlation between the GST and MIL predictions can be achieved by selecting a certain ROI size and an appropriate DTI_{thres} to distinguish regions where a reliable transverse isotropic direction can be computed. The DTI_{thres} can be calculated individually following a linear relationship for BMD, allowing for more regions to be assessed as transversely isotropic. Furthermore, a scaling parameter n was presented to achieve a 1:1 relationship between GST and MIL eigenvalues. Bone mechanical properties depend not only on BMD but also on trabecular morphology, and these results provide a step towards improving the predictions of femoral strength, failure load within different loading configurations with QCT-based FE models by providing a method for including transversely isotropic material information.

ACKNOWLEDGMENTS

The authors wish to thank Ms. Linda Ringqvist for help with illustrations.

CONFLICT OF INTEREST

There is no financial or personal conflict of interest with other people or organizations that could inappropriately influence the manuscript material and the authors work.

REFERENCES

[1]Christen, P., K. Ito, R. Muller, M. R. Rubin, D. W. Dempster, J. P. Bilezikian, and B. van Rietbergen. Patient-specific bone modelling and remodelling simulation of hypoparathyroidism based on human iliac crest biopsies. *J. Biomech.* 45(14):2411–2416, 2012.

[2]Cody, D. D., G. J. Gross, F. J. Hou, H. J. Spencer, S. A. Goldstein, and D. P. Fyhrie. Femoral strength is better predicted by finite element models than QCT and DXA. *J. Biomech.* 32(10):1013–1020, 1999.

[3]Consensus development conference. Prophylaxis and treatment of osteoporosis. *Am. J. Med.* 90(1):107–110, 1991.

[4]Cosmi, F. Morphology-based prediction of elastic properties of trabecular bone samples. *Acta Bioeng. Biomech.* 11(1):3–9, 2009.

[5]Cowin, S. C. The relationship between the elasticity tensor and the fabric tensor. *Mech. Mater.* 4(2):137–147, 1985.

[6]Dall'Ara, E., B. Luisier, R. Schmidt, F. Kainberger, P. Zysset, and D. Pahr. A nonlinear QCT-based finite element model validation study for the human femur tested in two configurations in vitro. *Bone* 52(1):27–38, 2013.

[7]Dragomir-Daescu, D., J. Op Den Buijs, S. McEligot, Y. Dai, R. C. Entwistle, C. Salas, L. J. Melton, III, K. E. Bennet, S. Khosla, and S. Amin. Robust QCT/FEA models of proximal femur stiffness and fracture load during a sideways fall on the hip. *Ann. Biomed. Eng.* 39(2):742–755, 2011.

[8]Fedorov, A., R. Beichel, J. Kalpathy-Cramer, J. Finet, J. C. Fillion-Robin, S. Pujol, C. Bauer, D. Jennings, F. Fennessy, M. Sonka, J. Buatti, S. Aylward, J. V. Miller, S. Pieper, and R. Kikinis. 3D Slicer as an image computing platform for the Quantitative Imaging Network. *Magn. Reson. Imaging* 30(9):1323–1341, 2012.

[9]Geraets, W. G., L. J. van Ruijven, J. G. Verheij, P. F. van der Stelt, and T. M. van Eijden. Spatial orientation in bone samples and Young's modulus. *J. Biomech.* 41(10):2206–2210, 2008.

[10]Harrigan, T. P., and R. W. Mann. Characterization of microstructural anisotropy in orthotropic materials using a second rank tensor. *J. Mater. Sci.* 19(3):761–767, 1984.

[11]Kang, Y., K. Engelke, and W. A. Kalender. A new accurate and precise 3-D segmentation method for skeletal structures in volumetric CT data. *IEEE Trans. Med. Imaging* 22(5):586–598, 2003.

[12]Kersh, M., P. Zysset, D. Pahr, U. Wolfram, D. Larsson, and M. Pandy. "Measurement of structural anisotropy in femoral trabecular bone using clinical-resolution CT images. *J. Biomech.* 46(15):2659–2666, 2013.

[13]Lenaerts, L., and G. H. van Lenthe. Multi-level patient-specific modelling of the proximal femur. A promising tool to quantify the effect of osteoporosis treatment. *Philos. Trans. R. Soc. A.* 367(1895):2079–2093, 2009.

[14]Liu, Y., P. K. Saha, and Z. Xu. Quantitative characterization of trabecular bone micro-architecture using tensor scale and multi-detector CT imaging. *Lect. Notes Comput. Sci.* 15(1):124–131, 2012.

[15]Matsuura, M., F. Eckstein, E. M. Lochmuller, and P. K. Zysset. The role of fabric in the quasi-static compressive mechanical properties of human trabecular bone from various anatomical locations. *Biomech. Model Mechan.* 19:19, 2007.

[16]Ohman, C., M. Baleani, E. Perilli, E. Dall'Ara, S. Tassani, F. Baruffaldi, and M. Viceconti. Mechanical testing of cancellous bone from the femoral head: experimental errors due to off-axis measurements. *J. Biomech.* 40(11):2426–2433, 2007.

[17]Pahr, D., and P. Zysset. A comparison of enhanced continuum FE with micro FE models of human vertebral bodies. *J. Biomech.* 42(4):455–462, 2009.

[18]Pahr, D. H., and P. K. Zysset. From high-resolution CT data to finite element models: development of an integrated modular framework. *Comput. Methods Biomech.* 12(1):45–57, 2009.
[19]Pahr, D., J. Schwiedrzik, E. Dall'Ara, and P. Zysset. Clinical versus pre-clinical FE models for vertebral body strength predictions. *J. Mech. Behav. Biomed.* 12:S1751–S6161, 2012.
[20]Pieper, S., M. Halle, and R. Kikinis. 3D SLICER. I S Biomed Imaging. Vol. 1, pp. 632–635, 2004.
[21]Pieper, S., W. Lorensen, W. Schroeder, and R. Kikinis. The NA-MIC Kit: ITK, VTK, Pipelines, Grids and 3D Slicer as an Open Platform for the Medical Image Computing Community. I S Biomed Imaging, Vol. 1, pp. 698–701, 2006.
[22]Ridler, T. W., and S. Calvard. Picture thresholding using an iterative selection method. *IEEE Trans. Syst. Man Cybern. B* 8(8):630–632, 1978.
[23]Rotter, M., A. Berg, H. Langenberger, S. Grampp, H. Imhof, and E. Moser. Autocorrelation analysis of bone structure. *J. Magn. Reson. Imaging* 14(1):87–93, 2001.
[24]San Antonio, T., M. Ciaccia, C. Müller-Karger, and E. Casanova. Orientation of orthotropic material properties in a femur FE model: a method based on the principal stresses directions. *Med. Eng. Phys.* 34(7):914–919, 2012.
[25]Scherf, H., and R. Tilgner. A new high-resolution computed tomography (CT) segmentation method for trabecular bone architectural analysis. *Am. J. Phys. Anthropol.* 140(1):39–51, 2009.
[26]Schulte, F. A., A. Zwahlen, F. M. Lambers, G. Kuhn, D. Ruffoni, D. Betts, D. J. Webster, and R. Muller. Strain-adaptive in silico modeling of bone adaptation—a computer simulation validated by in vivo micro-computed tomography data. *Bone* 52(1):485–492, 2013.
[27]Siris, E. S., P. D. Miller, E. Barrett-Connor, K. G. Faulkner, L. E. Wehren, T. A. Abbott, M. L. Berger, A. C. Santora, and L. M. Sherwood. Identification and fracture outcomes of undiagnosed low bone mineral density in postmeno-pausal women. *JAMA* 286(22):2815–2822, 2001.
[28]Tabor, Z. On the equivalence of two methods of determining fabric tensor. *Med. Eng. Phys.* 31:1313–1322, 2009.
[29]Tabor, Z. Anisotropic resolution biases estimation of fabric from 3D gray-level images. *Med. Eng. Phys.* 32:39–48, 2010.
[30]Tabor, Z. Equivalence of mean intercept length and gradient fabric tensors—3D study. *Med. Eng. Phys.* 34(5):598–604, 2012.
[31]Tabor, Z., and E. Rokita. Quantifying anisotropy of trabecular bone from gray-level images. *Bone* 40(4):966–972, 2007.
[32]Trabelsi, N., and Z. Yosibash. Patient-specific finite-element analyses of the proximal femur with orthotropic material properties validated by experiments. *J. Biomed. Eng.* 133(6):061001, 2011.
[33]Varga, P. Prediction of Distal Radius Fracture Load Using HR-pQCT-Based Finite Element Analysis. Vienna: Vienna University of Technology, 2009.
[34]Varga, P., and P. K. Zysset. Sampling sphere orientation distribution: an efficient method to quantify trabecular bone fabric on grayscale images. *Med. Image Anal.* 13(3):530–541, 2009.
[35]Wald, M. J., B. Vasilic, P. K. Saha, and F. W. Wehrli. Spatial autocorrelation and mean intercept length analysis of trabecular bone anisotropy applied to in vivo magnetic resonance imaging. *Med. Phys.* 34(3):1110–1120, 2007.
[36]WHO. Assessment of Fracture Risk and Its Application to Screening for Postmenopausal Osteoporosis. Geneve: WHO, 1994.
[37]Wolfram, U., B. Schmitz, F. Heuer, M. Reinehr, and H. J. Wilke. Vertebral trabecular main direction can be determined from clinical CT datasets using the gradient structure tensor and not the inertia tensor–a case study. *J. Biomech.* 42(10):1390–1396, 2009.
[38]Zysset, P. K., and A. Curnier. An alternative model for anisotropic elasticity based on fabric tensor. *Mech. Mater.* 21:243–250, 1995.